JACS
JOURNAL OF THE AMERICAN CHEMICAL SOCIETY
Article
pubs.acs.org/JACS

Interaction of Single-Stranded DNA with Curved Carbon Nanotube Is Much Stronger Than with Flat Graphite

Sara Iliafar,[†] Jeetain Mittal,[†] Dmitri Vezenov,*[,§] and Anand Jagota*[,†,‡]

[†]Department of Chemical and Biomolecular Engineering and [‡]Bioengineering Program, Lehigh University, Bethlehem, Pennsylvania 18015, United States

[§]Department of Chemistry, Lehigh University, 6. E. Packer Ave., Bethlehem, Pennsylvania 18015, United States

ABSTRACT: We used single molecule force spectroscopy to measure the force required to remove single-stranded DNA (ssDNA) homopolymers from single-walled carbon nanotubes (SWCNTs) deposited on methyl-terminated self-assembled monolayers (SAMs). The peeling forces obtained from these experiments are bimodal in distribution. The cluster of low forces corresponds to peeling from the SAM surface, while the cluster of high forces corresponds to peeling from the SWCNTs. Using a simple equilibrium model of the single molecule peeling process, we calculated the free energy of binding per nucleotide. We found that the free energy of ssDNA binding to hydrophobic SAMs decreases as poly(A) > poly(G) ≈ poly(T) > poly(C) (16.9 ± 0.1; 9.7 ± 0.1; 9.5 ± 0.1; 8.7 ± 0.1 k_BT, per nucleotide). The free energy of ssDNA binding to SWCNT adsorbed on this SAM also decreases in the same order poly(A) > poly(G) > poly(T) > poly(C), but its magnitude is significantly greater than that of DNA−SAM binding energy (38.1 ± 0.2; 33.9 ± 0.1; 23.3 ± 0.1; 17.1 ± 0.1 k_BT, per nucleotide). An unexpected finding is that binding strength of ssDNA to the curved SWCNTs is much greater than to flat graphite, which also has a different ranking (poly(T) > poly(A) > poly(G) ≥ poly(C); 11.3 ± 0.8, 9.9 ± 0.5, 8.3 ± 0.2, and 7.5 ± 0.8 k_BT, respectively, per nucleotide). Replica-exchange molecular dynamics simulations show that ssDNA binds preferentially to the curved SWCNT surface, leading us to conclude that the differences in ssDNA binding between graphite and nanotubes arise from the spontaneous curvature of ssDNA.

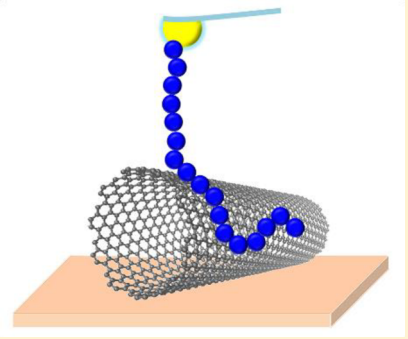

1. INTRODUCTION

The rich electrical, mechanical, and thermal properties of single-walled carbon nanotubes (SWCNTs) have made them strong candidates for a number of applications. For biomedical applications such as sensing,[1] drug delivery,[2] and medical nanorobots,[3] as well as for solution-based sorting and purification,[4] SWCNTs are usually dispersed in water by covalent, noncovalent, ionic, and free-radical modification of the surface of the SWCNTs.[5−7] Noncovalent functionalization of SWCNTs by amphiphilic molecules such as surfactants,[8,9] DNA,[4,10,11] and some peptides[12−14] has received significant attention because it permits ease of dispersion and processing without significantly affecting the intrinsic electronic structure of the SWCNTs.[15] Both for design of noncovalent functionalization strategies, and to establish a basis for understanding how nanomaterials such as SWCNTs interact with biological molecules, it is important to quantify the binding strength between SWCNTs and their dispersants.

Single molecule force spectroscopy (SMFS) has emerged as a powerful tool for the study of the mechanical behavior of individual molecules. It has been used to characterize elasticity,[16−18] DNA binding modes,[19−22] cell adhesion,[23−25] protein unfolding,[26−33] and colloidal forces.[34] It can also be used to measure the force required to remove an adsorbed molecule from a surface,[19−21,35−37] which can be useful for label-free biosensing.[38] In this case, long molecules are usually attached to an AFM probe, which is brought into contact with a substrate and then retracted with concurrent measurement of force and displacement. Depending on the nature of the force−displacement response, one can extract from it information regarding the elasticity of the molecule and/or its free energy of binding to the substrate. Often, a flat peeling force plateau is observed, which is followed by a force step corresponding to the detachment of the last, single, molecule from the surface. The height of the force step is used to calculate the free energy of binding of the molecule to the surface.[22,36,39]

Simulation studies of DNA near a surface coated with a self-assembled monolayer (SAM) of molecules show significant differences in adsorption thermodynamics depending on SAM structure.[40] Molecular dynamics simulations of DNA near a graphene surface show that adsorption of bases to the surface competes with interaction between them.[41] DNA adsorption onto the highly curved surface of carbon nanotubes in solution is highly dependent on DNA sequence and the characteristics of the SWCNT[42] leading to the formation of novel secondary structures.[43] We have previously used SMFS to measure the interaction between ssDNA and graphite.[35,36] We found that binding strength between ssDNA homopolymers could be ranked as poly(T) > poly(A) > poly(G) ≥ poly(C); with

Received: June 3, 2014
Published: August 27, 2014

   dx.doi.org/10.1021/ja5055498 | J. Am. Chem. Soc. 2014, 136, 12947−12957

corresponding free energies of 11.3 ± 0.8 k_BT, 9.9 ± 0.5 k_BT, 8.3 ± 0.2 k_BT, and 7.5 ± 0.8 k_BT per nucleotide. The peeling force for removing DNA from graphite has been reported to depend not only on the sequence but also on the hybridization state of the DNA (single-stranded versus double-stranded, perfect-match versus mismatched complement).[37,38] Both experimentally[22] and theoretically,[44,45] it has been shown that, over a broad range of rates, peeling occurs under equilibrium such that measured force can be related to free energy of desorption.

Here, we report on work in which we applied SMFS to study the interaction of ssDNA homopolymers 5′-poly(T_{100}), 5′-poly(G_{100}), 5′-poly(A_{100}), and 5′-poly(C_{100}) (5′-terminus is attached to the force probe) with SWCNTs adsorbed onto a surface coated by a methyl-terminated SAM. We show that the force required to peel ssDNA off the SAM is distinctly different from that required to peel it off an SWCNT. Moreover, we report a surprising finding that binding strength of ssDNA to the curved SWCNTs is much larger than to flat graphite. We have conducted replica-exchange molecular dynamics (REMD) to show that ssDNA binds preferentially to the curved SWCNT surface and used results of these simulations to interpret the experimental observations.

2. EXPERIMENTAL SECTION

In order to measure the force required to peel a molecule off the surface of an SWCNT, we followed a multistep experimental routine that consisted of (i) preparing samples with individually dispersed SWCNTs, (ii) depositing them on a methyl-terminated SAM on a silicon wafer, (iii) removing the dispersant molecule off the SWCNT surface, and (iv) carrying out peeling experiments on the exposed SWCNTs. We also describe procedures used to conduct molecular dynamics simulations in order to aid interpretation of experimental findings.

2.1. Uniform Dispersions of 5′-$(GT)_3$-3′/(6,5) SWCNTs. Raw (6,5)-rich (>80%) semiconducting CoMoCAT carbon nanotubes (diameter of 0.7−0.9 nm) were obtained from South West NanoTechnologies (SWeNT). Single-stranded DNA 5′-$(GT)_3$-3′ was purchased from Integrated DNA Technologies, Inc. (Coralville, IA). Using a previously described procedure,[11,46] SWCNTs were dispersed with 5′-$(GT)_3$-3′ in a 1:1.5 (mass) ratio in 10 mM phosphate buffer (pH 7) containing 0.3 mM EDTA. This ssDNA sequence was chosen to be long enough to provide sufficient binding strength to disperse the SWCNTs effectively, but to be short enough to prevent DNA from wrapping around the SWCNTs. A sequence with the latter characteristic was selected in an effort to ease the postdispersion removal of DNA from the SWCNTs. The mixture was sonicated for 90 min in an ice bath at 8 W using a Branson probe sonicator (Sonifier 150, G. Heinemann, Germany). The dispersion was then centrifuged at 13 200 rpm for 90 min in order to separate the supernatant from residual undispersed SWCNTs (discarded as a pellet).

2.2. Formation of Hydrophobic Methyl-Terminated Self-Assembled Monolayers (SAMs) on Silicon Wafers. Silicon wafers (500 μm thickness, 3 in. diameter, 1−20 ohm·cm resistivity, N-type phosphorus doped, ⟨100⟩ crystal orientation) were purchased from Silicon Quest International (Santa Clara, CA). Organic contaminants were removed from the surface of these wafers by placing them in piranha solution (70% H_2SO_4 and 30% H_2O_2 by volume) for 30 min. The surfaces were then immediately modified by forming a hydrophobic monolayer of octyldimethylchlorosilane (ODMClSi) following a previously described procedure.[46,47] Briefly, the functionalization step was carried out by refluxing 9% (vol) ODMClSi in heptane and 1% (vol) butylamine in a pyrex crystallization dish at 60−65 °C for 3 h. Upon the completion of the chemical modification process, the samples were rinsed with isopropanol and annealed at 110 °C under nitrogen atmosphere for 2 h. The SAM-coated silicon wafers were later cut into smaller pieces (1 cm × 1 cm) for handling purposes. The hydrophobicity of these surfaces was characterized by measurements of advancing and receding contact angles of water, which were found to be 94 ± 3° and 89 ± 4°, respectively. The thickness of the SAM determined by ellipsometry (VASE, J.A. Woollam Co.) was 6.6 ± 0.3 Å.

2.3. Deposition of SWCNTs on Hydrophobic SAM. A 150 μL droplet of 90 μg/mL sample of dispersed 5′-$(GT)_3$-3′/(6,5) SWCNTs was deposited on SAM-coated silicon wafers, allowed to remain in contact with the substrate for a prescribed duration (typically 10 min), and removed by aspiration with a pipet.[46] This procedure results in deposition of a submonolayer of individual SWCNTs on the substrate.[46] The topology of these surfaces was imaged using a Veeco Dimension V atomic force microscope (AFM) (Santa Barbara, CA).

2.4. Displacement of 5′-$(GT)_3$-3′ from the Surfaces of SWCNTs Using Sodium Dodecyl Benzenesulfonate (SDBS). We used a surfactant, SDBS, to remove the DNA from the SWCNTs adsorbed on the surface of hydrophobic silicon wafers. To establish that the SDBS indeed rapidly removes the DNA from SWCNTs, we conducted separate experiments in bulk solution phase. In this procedure, the absorbance spectrum of 100 μL of SWCNTs dispersed by ssDNA was measured using a UV−vis−NIR spectrophotometer (Varian Cary 50). To displace the ssDNA molecules, 0.2% (wt) solution of SDBS in 10 mM phosphate buffer (with 0.3 mM EDTA) was added to the ssDNA/SWCNT dispersion in a 1:1 ratio (vol). To monitor the DNA−SDBS exchange, the shift in the position of the absorbance peak from 990 to 978 nm was followed over time until SDBS had completely replaced ssDNA molecules from the SWCNTs.[48]

To remove DNA from the SWCNTs adsorbed on the solid surfaces, we immersed the samples into the same 0.2% (wt) SDBS solution for 2 min followed by rinsing with DI water. The samples were then dried with nitrogen. To obtain both a high coverage of SWCNTs on the surface and to displace ssDNA completely, we repeated the 5′-$(GT)_3$-3′/(6,5) SWCNTs deposition and SDBS/DI rinsing step three times. Control samples for analysis of surface chemical composition were prepared following the same procedure as described above except that, for the deposition step, we used a solution that contained no DNA-dispersed SWCNTs. For evidence of DNA removal by the SDBS solution, we carried out height analysis on AFM topography images of adsorbed SWCNTs captured between each step of the deposition and rinsing process.

We next used X-ray photoelectron spectroscopy (XPS) (Scienta ESCA-300) to scan for the presence of nitrogen on the substrate. The samples were positioned at a 20° takeoff angle between the sample surface and the path to the analyzer. Spectra were analyzed using CASA XPS software (version 2.3.15dev77). Survey spectra were taken at a 300 eV pass energy and with a step energy of 1 eV. The pass energy for high-resolution spectra in the N 1s region was 150 eV, and the step energy was 0.05 eV. Since, in our system, only ssDNA contains nitrogen, the existence or disappearance of this peak upon rinsing with SDBS indicates presence or absence, respectively, of DNA on the substrate.

2.5. Single-Molecule Peeling Experiments. Gold-coated atomic force microscopy (AFM) probes with nominal spring constant of 0.3 N/m (ContGB probes, Budget Sensors, Inc., Sofia, Bulgaria) were used in all SMFS experiments with the exception of one experiment in which the force measurements were coupled with imaging done using the same probe. For the latter experiment, we used a gold-coated probe having nominal stiffness 3.5 ± 1.5 N/m (NSC18 probes, MikroMasch, San Jose, CA). The probe for imaging was chosen empirically from several models as the one providing images of CNTs in fluid that were of acceptable quality and not showing signs of nanotube displacement in the course of imaging.

The force probes were cleaned by exposure to air plasma (PDC-001 plasma cleaner, Harrick Plasma, Ithaca, NY) for 1 min on high power, and rinsed with ethanol. 5′-Thiol-modified DNA (purchased from Integrated DNA Technologies, Inc.) was dissolved at 0.1 nM concentration in a 10 mM phosphate buffer with 1 M ionic strength

NaCl (pH ~7). To deprotect the thiol group, TCEP (tris(2-carboxyethyl)phosphine, 98% purity, purchased from Alfa Aesar, Ward Hill, MA) was added to the DNA solution (to obtain 6 mM concentration), and this solution was then left for 30 min to allow ample time to reduce the disulfide. Next, the Au-coated AFM tips were placed in the ssDNA solution for 1 h. The chemically functionalized AFM probe was then placed in a 6 mM solution of mercaptohexanoic acid (MHA) in ethanol for 1 h to space out the ssDNA molecules by filling the remaining sites on the surface of the gold-coated tip and to remove nonspecifically adsorbed DNA. The probe was rinsed with ethanol and dried with nitrogen after each modification step. A characteristic behavior inherent to the force–distance relationship is an adhesive force required to break the contact between the decorated probe and the substrate during retraction; it is important to design the experiment such that this adhesive force not be so large as to completely mask the force plateau, which occurs subsequently. Use of MHA resulted in the negatively charged hydrophilic probe surface that we found helpful in reducing initial pull-off force due to nonspecific adhesion and presence of multiple ssDNA molecules on the probe tip. The initial adhesion varied from probe to probe and was typically in the range 1–10 nN. In the experiment with simultaneous imaging and force measurements, adhesion at initial tip pull-off was as high as 30 nN, but because in this experiment the probe used was much stiffer than in all other experiments, the larger initial adhesion force did not significantly obscure the peeling region.

Using an MFP-3D atomic force microscope (Asylum Research, Santa Barbara, CA), single molecule (SM) peeling experiments were carried out in approximately 3 mL of 10 mM phosphate buffer containing 100 mM NaCl at room temperature (nominally 300 K). Following a previously established procedure,[36] the AFM cantilevers were calibrated in air after the completion of single molecule force spectroscopy (SMFS) experiments conducted in fluid. Because the surface consisted of SWCNTs adsorbed onto a methyl-terminated SAM, any particular experiment could represent peeling the molecule off an SWCNT or the SAM. To correlate a peeling experiment with the location off which the molecule was peeled, in one experiment, we first imaged the surface under tapping mode in fluid immediately prior to the peeling experiments. Next, we acquired a force–volume map, i.e., force–distance measurements obtained in a 2-dimensional array from the same area of the sample for which the topography image was just obtained. As described later in the paper, the distribution of peeling forces was found to be bimodal, with one cluster corresponding to peeling off the SAM and the other to peeling off SWCNTs. The peeling experiments were carried out at a scan rate of 200 nm/s. Maximum compressive force applied was less than 1 nN.

Figure 1 shows a typical force–distance relationship obtained for our steady state peeling process. In analyzing the force curves, we considered only the jump in the final peeling plateau, and used a custom code written in IGOR Pro (Wavemetrics, Eugene, OR) to obtain an average force measured over a distance of 2 nm on both sides of the molecule detachment step. We followed our previously established guidelines to identify valid force curves that were suitable for further analysis.[36] The peeling curves were considered to be valid if (i) the approach and retraction traces overlapped for the noncontact region, (ii) the separation distance of the last peeling step was smaller than that of the DNA contour length, (iii) the tip–surface adhesion was small enough that the peeling steps were not masked by the initial pull-off force, and (iv) the peeling region displayed a flat plateau for at least 10 nm of separation to present a steady state peeling process.[36] All measurements reported in this paper are mean values; errors indicate 95% confidence limits obtained from averaging peeling forces from multiple force–distance curves obtained in several independent experiments (at least in triplicates using different probes) that were carried out under nominally identical conditions.

2.6. Molecular Simulation. To probe at the molecular level the structural differences of the system when an ssDNA molecule interacts with different surfaces, we conducted a set of replica exchange molecular dynamics (REMD) simulations in the canonical ensemble. REMD simulations were used to obtain robust configurational sampling by conducting the simulation at the temperature of interest

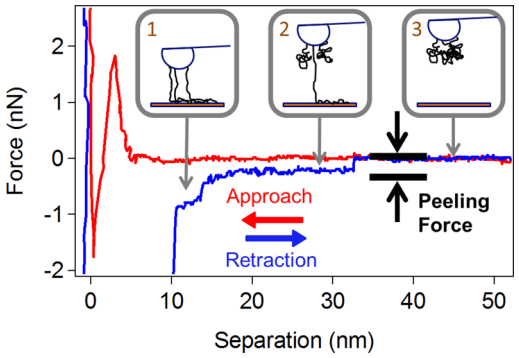

Figure 1. Typical force–distance curve for peeling 5′-T_{100} ssDNA from SWCNTs deposited on a methyl-terminated SAM on a silicon wafer. The force curves were obtained at a tip velocity of 200 nm/s in 10 mM phosphate buffer containing 100 mM NaCl. The red curve is for the tip approaching the surface; the blue curve represents tip retraction. This curve was obtained with the same tip that was used to generate the topographical image shown in Figure 7. As the AFM probe approaches the surface, the electrical double layer and steric forces give repulsive interactions. When the ssDNA strands eventually find the substrate, a jump-to-contact is observed. On retraction, the adhesive interactions between multiple ssDNA molecules and the substrate, as well as nonspecific interactions between groups on the AFM tip and the surface, result in a large initial pull-off force. Upon further retraction, a few remaining strands keep the AFM probe connected to the surface (1). Continuing the removal process eventually leaves only a single strand attached to the surface (2). In the last stage, further retraction from the surface leads to the detachment of the final strand (3). The force jump from this final stage is used in our model to extract the adhesion free energy between the ssDNA and the substrate.

as well as at higher temperatures, enabling the system to easily overcome energy barriers that separate the various conformational states.[49] Because the adsorption free energy is about 10 k_BT per base, it is not feasible even with extensive REMD simulation to obtain equilibrium ensembles of adsorbed versus desorbed structures. However, because barriers for lateral motion of adsorbed structures are relatively small, REMD allows essentially complete sampling of various adsorbed conformations, yielding robust information about equilibrium adsorbed ensembles. The number of water molecules in the simulation box was adjusted initially to obtain pressure normal to the surface (SAM or graphite) close to 1 bar. The temperature range used in our REMD simulations was 300–585 K with a total of 48 replicas. The replica temperatures were chosen to maintain the exchange acceptance ratios at about 10–20% with an exchange time of 1 ps. The time step of the simulation was 2 fs with a total simulation run of 200 ns. We used the GROMACS 4.5.3[50] simulation package, the CHARMM27 force field for nucleic acids,[51] and TIP3P water[52] in our REMD simulations. The SAM surfaces were constructed on the basis of previous work by Garde and co-workers[53] to match the surface hydrophobicity of various head-groups.[54] Here, we used SAM surfaces with CH_3 head-groups represented in all-atom detail connected to alkyl chains (C10) represented by a united-atom model for alkanes. The last atom of the alkyl chain in both directions was bonded to a sulfur atom which was frozen during the simulation. That is, we created a SAM bilayer exposing two CH_3 terminated surfaces. The SWCNT atoms were modeled by the sp2 hybridized atom type in CHARMM27 consistent with previous work.[55] The ssDNA sequence used was poly(T_{12}), and the SWCNT was a (6,5) nanotube with a length of 40.58 Å and diameter of 7.47 Å. The system was solvated in a periodic rectangular water-box, containing approximately 17 000 total atoms, of which 4000 were water molecules with 11 sodium counterions to balance the negative phosphate charges. The system dynamics was propagated using the leapfrog integrator, and constant temperature was maintained using the Nose-Hoover thermostat[56,57]

dx.doi.org/10.1021/ja5055498 | J. Am. Chem. Soc. 2014, 136, 12947–12957

with a time constant of 1 ps. Electrostatic interactions were calculated using the particle mesh Ewald (PME) method[58] with a real space cutoff value of 9 Å. We used a 12 Å cutoff value for van der Waals interactions. Out of the 200 ns total simulation time, we discarded the first 50 ns as equilibration and used data from the remaining 150 ns run for further analysis presented in this paper. System configurations were saved every 10 ps and used to obtain density profiles. To obtain information about stable equilibrium conformations, we used structural clustering using the GROMOS method[59] with a cutoff distance of 3 Å based on DNA backbone heavy atoms. We used 1500 configurations saved every 100 ps for this analysis.

3. RESULTS AND DISCUSSION

3.1. Bare Carbon Nanotubes on a Hydrophobic Self-Assembled Monolayer. Prior to conducting force measurements, it is necessary to establish that the DNA has been removed from SWCNTs adsorbed on the silicon wafer. DNA was removed by rinsing samples with a solution of an ionic surfactant, SDBS. The surfactant, in turn, was removed by rinsing with DI water. We first show that this surfactant is effective in removing DNA off the surface of dispersed SWCNTs. Figure 2 shows absorbance spectra of DNA-coated SWCNTs before and after addition of SDBS at ambient temperature. We have shown previously that DNA-coated SWCNTs have a characteristic absorbance peak at 990 nm, whereas SDBS-coated SWCNTs have a peak at 978 nm.[46,48] Figure 2 demonstrates that the displacement of 5′-$(GT)_3$-3′ by SDBS is very rapid at room temperature.

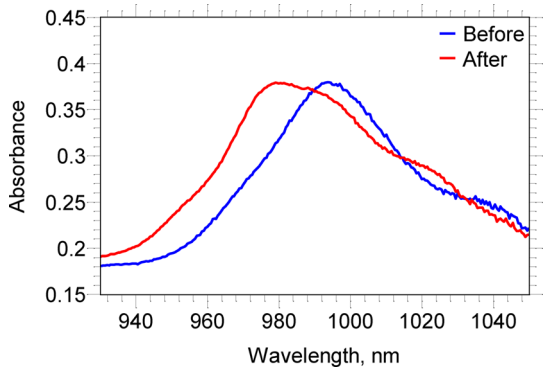

Figure 2. Peak position of the NIR absorbance spectrum of the SWCNT dispersion shifts from 990 nm (DNA-coated) to 978 nm (SDBS-coated) immediately upon addition of the SDBS solution. Subsequent scans obtained 10 min after the addition of SDBS to the 5′-$(GT)_3$-3′/SWCNT dispersion showed no further change. This experiment was repeated three times to ensure reproducibility of the results.

To obtain bare SWCNTs, samples with adsorbed nanotubes were subjected to rinsing by SDBS solution followed by rinsing with DI water. We used several deposition−rinse cycles to increase the density of the nanotubes on the surface. Between each step in the process, the topography of these samples was imaged in air. To obtain the average SWCNT diameters, we subtracted the baseline from the image, identified areas predominantly covered with individual SWCNTs rather than bundles (maximum height of less than 1.6 nm), zoomed into these areas (as shown in Figure 3), and used a built-in depth analysis tool (Veeco) to determine the average diameter of the SWCNTs. This analysis tool compiles a histogram of depth data within the specified area, where depth is the difference in height between the highest point found in the image and the height of a given pixel. The analysis tool then applies a Gaussian low-pass filter to the data to remove noise, and compares the heights between two dominant features by automatically finding the mean of each distribution and calculating the peak-to-peak distance, i.e., the difference in height. In our studies, we obtained one height distribution for the SAM-coated silicon wafer and another for the SWCNTs (Figure 3C). To measure the height of the SWCNTs, the difference between the height of the background substrate and that of the SWCNTs was calculated. Furthermore, we independently checked and confirmed the values obtained via the depth analysis tool by manually measuring changes in height over the cross-section of SWCNTs deposited on the SAM for multiple samples. The average diameters (each obtained from over 300 or more image height histograms) showed a gradual decrease from the first deposition of the nanotubes to the last DI water rinsing step (Figure 4). Quantitatively, the measured diameters decreased from 1.4 ± 0.20 nm (19 samples) after the first SWCNT deposition to 0.85 ± 0.06 nm (35 samples) after the last rinsing step. Since the diameter of these SWCNTs as reported by the manufacturer (Sigma-Aldrich Corp) is 0.7−0.9 nm, our height analysis results evidently support the interpretation that SDBS rinsing replaces 5′-$(GT)_3$-3′ from the surface of SWCNTs, while the follow-up rinsing with DI water removes SDBS from the SWCNTs.

Figure 4 shows that each SDBS/water rinsing step reduces the average SWCNT height by 0.2−0.3 nm, consistent with the removal of DNA. Following the subsequent deposition step, the height increases only slightly. Khripin et al. have shown that the deposition of DNA-CNT on a SAM substrate is highly dependent on the density of previously deposited SWCNTs on that substrate.[46] In particular, they have reported that the random sequential adsorption approaches a saturation density, which likely limits how much the height can increase during subsequent depositions. Notice that average SWCNT height after each SDBS/water rinse continues to decrease. This observation could be due to a number of reasons, e.g., (i) because DNA is incompletely removed in a single rinse step and repeated rinsing is required to improve efficiency, (ii) SDBS rinsing selectively removes larger diameter SWCNTs, or (iii) rinsing breaks down small bundles of nanotubes or crossing nanotubes.

To investigate further whether the SDBS rinse fully removed the ssDNA from the surface of the previously deposited SWCNTs, we carried out an XPS study of the surface chemical composition. Following the same deposition-and-rinse procedure as described earlier, now with two cycles instead of three, we prepared the following three samples using SAM-coated silicon wafers: (i) a control sample exposed to phosphate buffer (no rinse step), (ii) a dispersion of 5′-$(GT)_3$-3′-coated SWCNTs deposited without the rinse step, and (iii) a dispersion of 5′-$(GT)_3$-3′-coated SWCNTs deposited and rinsed with the SDBS/DI water. Since ssDNA is the only component in our system that contains nitrogen, we scanned for the presence of nitrogen in our samples.

Figure 5 shows a high-resolution XPS spectrum of N 1s region obtained from these three samples. The disappearance of the N 1s peak after the second SDBS/DI water rinse cycle observed here further supports our finding from the AFM height analysis that this rinsing step completely removes all ssDNA from the surface of carbon nanotubes deposited on the SAM substrate. Moreover, we found that this N 1s peak is best fitted with two Gaussian components, suggesting that the

dx.doi.org/10.1021/ja5055498 | J. Am. Chem. Soc. 2014, 136, 12947−12957

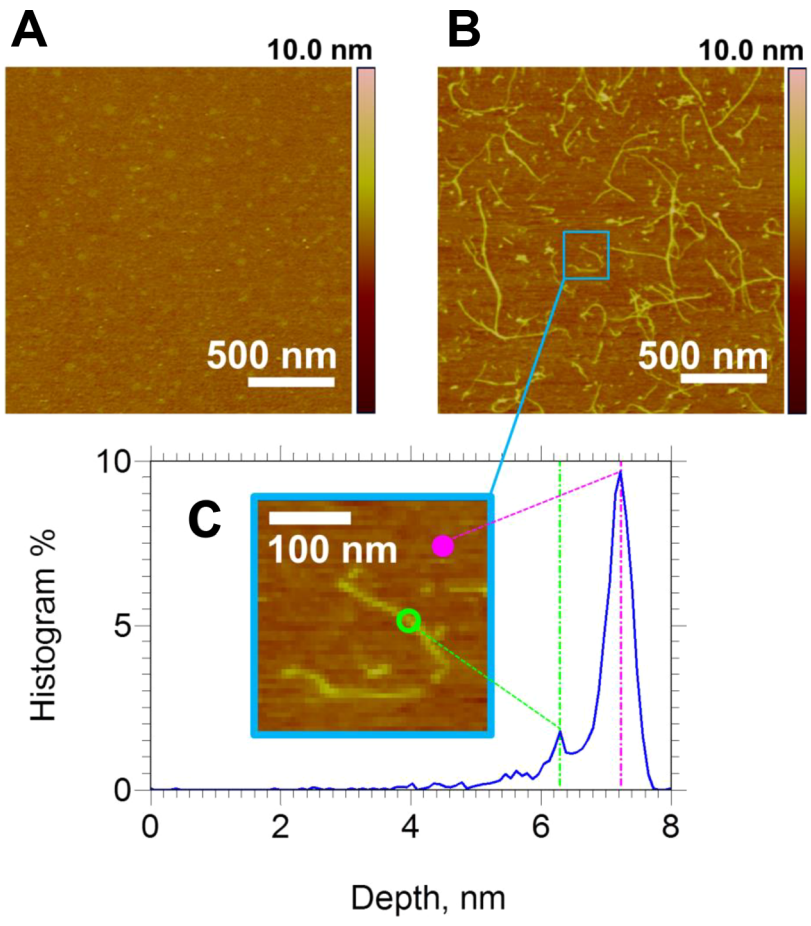

Figure 3. Surface topography of SAM-coated silicon wafers obtained in air for (A) a control sample exposed to phosphate buffer only, and (B) a sample exposed for 10 min to a droplet of 90 μg/mL dispersion of 5′-$(GT)_3$-3′-coated SWCNTs and then rinsed by SDBS (2 min) and DI water. The sample in part B had undergone three CNT-deposition−surfactant/water−rinse cycles. (C) Using the depth analysis tool, height distributions for the SWCNTs (as indicated by the green open circle) as well as the background SAM-coated silicon surface (represented by the purple closed circle) were obtained. In part C, the abscissa is labeled as "depth" because it represents the height distance between the tallest feature in the sample and any other point. The diameter of the SWCNTs was then calculated as the distance between the two peaks of the depth distribution, averaged over multiple areas and samples.

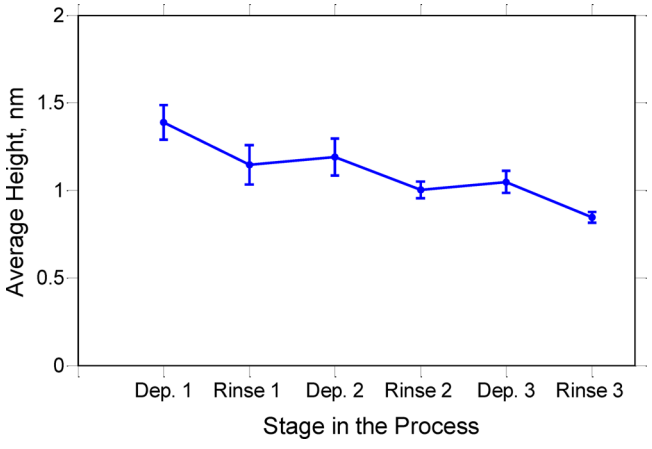

Figure 4. Analysis of the average height of the nanotubes after each step of 5′-$(GT)_3$-3′/SWCNT deposition and SDBS/DI water rinse showed a gradual decrease in the apparent mean diameter of the CNTs. After the third rinsing step, the mean diameter of 0.85 ± 0.06 nm (35 separate measurements) is well within the diameter range (0.7−0.9 nm) of bare SWCNTs reported by the manufacturer.

nitrogen has two distinct chemical environments, consistent with the ssDNA composition, 5′-$(GT)_3$-3′. To obtain the fits, we restricted the full width at half-maximum (fwhm) of the two peaks to be the same. An XPS study conducted by Ptasinka et al. on DNA nucleobases deposited on untreated silicon wafers has shown that thymine's N 1s peak is best fitted with one Gaussian peak located slightly above 400 eV, while guanine's nitrogen peak is best fitted with two Gaussian components.[60] The first Gaussian component of guanine's N 1s peak is located at the same binding energy as that of thymine's N 1s peak, and its second component is positioned at a slightly lower energy, around 399 eV.[60] In their paper, Ptasinka et al. attributed the higher energy peak to amino (C—NH—C and C—NH_2) sites, while they associated the lower energy peak with the imino (C—N═C) species.[60] Following Ptasinka's interpretation, we obtained a two-component Gaussian fit for our sample containing $(GT)_3$. Here, we found that the ratio of the area for the high energy peak to that of the low energy one was, not surprisingly, 5:2, corresponding to five amino sites and two imino sites in the GT repeat unit. Since the complete removal of ssDNA from the substrate is evident from our XPS study, we attribute the small gradual decrease in SWCNT height with the number of SDBS rinsing steps to be due to the breakup of small bundles.

dx.doi.org/10.1021/ja5055498 | J. Am. Chem. Soc. 2014, 136, 12947−12957

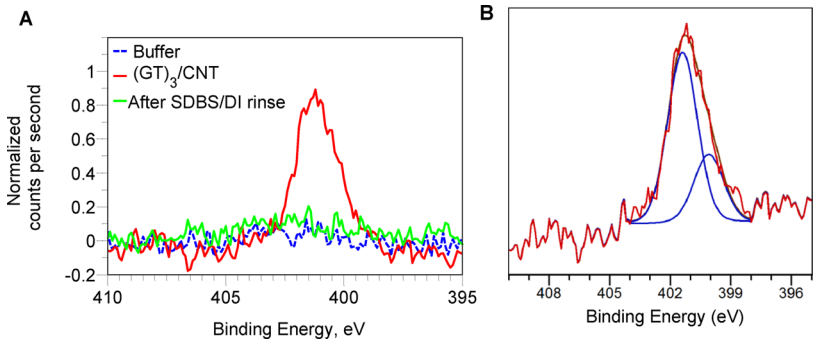

Figure 5. (A) High resolution XPS spectra of the N 1s region obtained for three samples with the following variations in the preparation: (i) a sample exposed to buffer (no DNA) without the rinse step, (ii) a dispersion of 5′-$(GT)_3$-3′/SWCNT deposited without the rinse step, and (iii) a dispersion of 5′-$(GT)_3$-3′/SWCNT deposited, followed by the SDBS/DI water rinse. The SAM-coated silicon wafer on which a dispersion of 5′-$(GT)_3$-3′/SWCNT was deposited without the rinse step displayed a peak located at 401.2 eV with fwhm of 2.02 eV. (B) The N 1s peak from sample ii in part A can be represented by the superposition of two Gaussian components.

3.2. Peeling of Homopolymer ssDNA from Bare Single-Walled Carbon Nanotubes. To quantify the interaction between ssDNA homopolymers and SWCNTs, T_{100}/MHA functionalized gold-coated AFM force probes were first used to image a 3 μm × 3 μm area, where the SWCNTs were deposited on methyl-terminated SAMs. The same force probe was then used to obtain a force map from the same region. The term force map refers to an array of force−distance measurements (Figure 1) obtained over a selected area with a specified number of gridpoints (40 × 40 in our experiments). Given the much larger size of the CNT compared to DNA we do not expect rolling or sliding of the CNT during peeling even if the DNA can be forced to slide more or less freely. The fact that CNT remained on the surface in the course of extensive washing (hydrodynamic drag plus meniscus forces) implies that CNTs are pinned to the surface.

The peeling forces measured from a typical force map acquired with a T_{100}-modified probe were plotted as a histogram and revealed two distinct force peaks (similar to those shown in Figure 6A). Using Igor's multipeak fitting package, we fitted two Gaussian distributions to our bimodal peeling force data and obtained mean peeling forces of 78.4 ± 0.8 pN (total of n = 1673 valid force curves) and 172.0 ± 1.6 pN (n = 714). We have previously reported that the peeling of polythymine from a methyl-terminated SAM prepared under the same conditions as used for this study results in 77.5 pN mean peeling force.[36] This comparison suggests that the first peak in the histogram corresponds to peeling ssDNA from the SAM, whereas the second peak should then correspond to peeling ssDNA from the SWCNT. Figure 6A−D shows a compilation of the results from analysis of all our experiments conducted using the four ssDNA homopolymers on SAM surfaces with bare SWCNTs. All force histograms display two distinct clusters: (i) low peeling forces with mean values similar across all sequences (70−130 pN), and (ii) high peeling forces with mean values covering a broader range of forces (130−260 pN).

We associate the first peak in the force histograms with the DNA−SAM interactions and the second peak with the DNA−nanotube interactions on the basis of the following three pieces of evidence (discussed in more detail below): (i) high peeling forces are localized in the nanotube-occupied regions, and low peeling forces are detected in the nanotube-free regions; (ii) bare SAM surfaces lacking the CNTs show a single peak in force histograms whose position is identical to that of the first

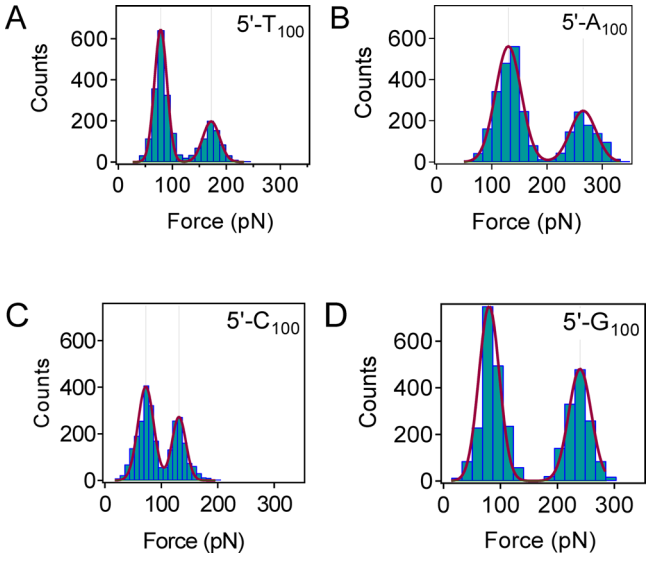

Figure 6. Force histograms for peeling ssDNA homopolymers from SWCNTs dispersed on a methyl-terminated SAM showing two distinct peaks (peak positions and errors of the mean are derived from the Gaussian fits to the experimental data). The distributions of peeling forces were centered at 78.4 ± 0.8 pN (total of n = 1673 force curves) and 172.0 ± 1.6 pN (n = 714) in 4 independent experiments for 5′-T_{100} (A), 130.0 ± 1.5 pN (n = 1948) and 265.4 ± 2.2 pN (n = 890) in 3 independent experiments for 5′-A_{100} (B), 72.5 ± 0.9 pN (n = 1863) and 131.2 ± 1.1 pN (n = 1114) in 3 independent experiments for 5′-C_{100} (C), and 80.1 ± 1.2 pN (n = 1879) and 239.8 ± 1.5 pN (n = 1339) from 3 independent experiments for 5′-G_{100} (D).

peak in the force histograms obtained from the SWCNT-on-SAM samples; (iii) the relative frequency of low versus high forces (ratio of histogram peak areas) tracks the relative surface coverage of CNTs and SAM as sensed by the AFM probe.

To confirm the assignment of the peaks, we correlated the spatial distribution of the high and low peeling forces with local sample composition. By considering the midpoint between peaks as a cutoff between the two force distributions, we assign a peeling force less than 127 pN to belong to the first peak in the histogram and a peeling force larger than 127 pN to belong to the second peak. We overlaid the locations of the sites where valid peeling force curves were obtained with the AFM height image (Figure 7). In Figure 7, we represent the location of a low force by a blue marker and the location of a high force by a

dx.doi.org/10.1021/ja5055498 | J. Am. Chem. Soc. 2014, 136, 12947−12957

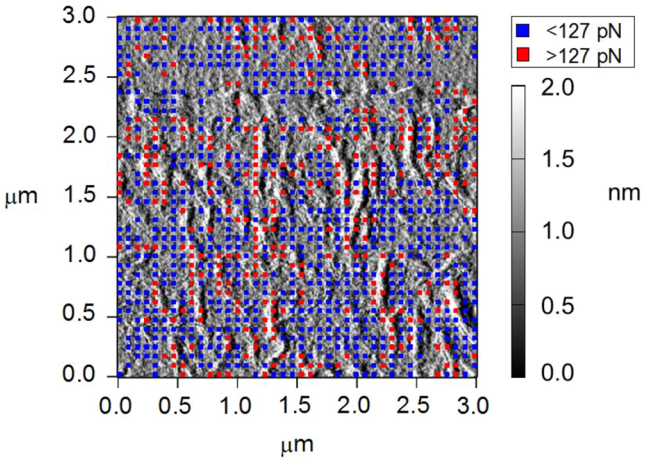

Figure 7. Superposition of the sample topography and locations of the gridpoints where individual force−distance curves were acquired from SWCNTs and a methyl-terminated SAM. Placement on the sample of valid force curves with the peeling force of less than 127 pN is shown by blue squares, and placement of force curves higher than 127 pN is shown in red. Despite some mismatch, there is a clear correlation between the location of the SWCNTs and the high peeling forces, and between the location of regions presenting methyl-terminated SAM and low peeling forces. In particular, the nanotubes are aligned vertically by the meniscus of the drop from which they were deposited, and the points of high force are likewise lined up vertically. As a simple statistical test, we estimated the probability that the neighbor of a high force point would be in the vertical versus the horizontal direction. A perfectly random arrangement would yield a value of 0.5 for each direction; we find that (sample size of 1289) the probability of a neighbor being in the vertical direction is 0.63 versus 0.37 in the horizontal direction.

red marker. It is clear that low forces identified as due to peeling from the SAM coated surface correspond well with regions of the image between SWCNTs. On the contrary, high forces identified as due to peeling from the SWCNT correlate well with regions of the image where the SWCNTs lie. This placement of high peeling forces in the vicinity of the nanotubes supports the interpretation that the high peeling forces are due to removal of T_{100} ssDNA from individual SWCNTs.

By carrying out experiments on peeling ssDNA from SAM-coated silicon wafers lacking the nanotubes, we observed a single-mode distribution of peeling forces: 125.1 ± 3.5 pN for poly(A) (3 experiments with n = 116 valid force curves), 74.2 ± 0.8 pN for poly(C) (4 experiments, n = 844), and 77.0 ± 1.9 pN for poly(G) (3 experiments, n = 316). Note that we previously reported 77.5 pN mean peeling force for poly(T), also producing a single-mode force distribution. Since in the presence of deposited nanotubes a bimodal distribution of forces is observed reproducibly for all ssDNA homopolymers, and considering that the low-force mode was found to be similar to peeling from the bare SAM, we have interpreted the higher forces to be due to the interactions of the ssDNA with the carbon nanotubes.

Finally, we note that it is not surprising that the probability that the peeling force falls into the distribution peak arising from the DNA−SWCNTs interaction is always lower than that associated with the SAM (compare peak areas in Figure 6A−D). To corroborate this observation, we examined the surface coverage of SWCNTs on 34 independent SAM-coated silicon wafers with concentration of deposited SWCNTs typical of the sample preparation for the peeling experiments (i.e., deposition from 90 μg/mL solution). Since the radius of AFM probes is 1−2 orders of magnitude larger than the diameter of the SWCNTs, the surface fraction of CNTs and contact area available for ssDNA−CNT interactions are both effectively increased due to convolution with the tip shape (and multiple DNA molecules available for binding with CNT). The height image shows CNTs much wider than ∼1 nm expected diameter. At the same time, long oligonucleotide (100-mers) at multiple attachment points near tip apex can interact with CNTs even when the probe is misaligned from the CNT axis. The ratio of SWCNTs to SAM on the substrates was found to be 1 to 5.0 ± 0.9. This finding indirectly supports our conclusion that high forces are due to peeling from SWCNTs, while the weak interactions are coming from ssDNA peeling from the SAM substrates.

The results shown in Figure 7 are summarized in Table 1. In our previous work, we demonstrated that a simple equilibrium

Table 1. Summary of the Peeling Forces and the Free Energy of Binding per Nucleotide for All ssDNA Homopolymers Interacting with Methyl-Terminated SAM or SWCNT

	SAM		SWCNT	
sequence	peeling force (pN)	binding energy per nucleotide (k_BT)	peeling force (pN)	binding energy per nucleotide (k_BT)
Pyrimidines with SAM-Coated Silicon Wafer as Substrate				
5′- poly(T_{100})	77.8 ± 1.6	9.4 ± 0.1		
5′- poly(C_{100})	74.2 ± 0.8	8.9 ± 0.1		
Purines with SAM-Coated Silicon Wafer as Substrate				
5′- poly(A_{100})	125.1 ± 3.5	16.2 ± 0.3		
5′- poly(G_{100})	77.0 ± 1.9	9.3 ± 0.1		
Pyrimidines with SWCNT Deposited on SAM-Coated Silicon Wafer as Substrate				
5′- poly(T_{100})	78.4 ± 0.8	9.5 ± 0.1	172.0 ± 1.6	23.3 ± 0.1
5′- poly(C_{100})	72.5 ± 0.9	8.7 ± 0.1	131.2 ± 1.1	17.1 ± 0.1
Purines with SWCNT Deposited on SAM-Coated Silicon Wafer as Substrate				
5′- poly(A_{100})	130.0 ± 1.5	16.9 ± 0.1	265.4 ± 2.2	38.1 ± 0.2
5′- poly(G_{100})	80.1 ± 1.2	9.7 ± 0.1	239.8 ± 1.5	33.9 ± 0.1

model can relate the peeling force f of a freely jointed chain (FJC) to free energy required to desorb a link from its adsorbed state on the surface to its desorbed state in solution, γ':[36,61]

$$\Gamma' = \ln\left[\frac{\sinh(F)}{F}\right] \quad (1)$$

where $\Gamma' = ((\gamma' b)/(k_BT))$ is the dimensionless free energy and $F = ((f b)/(k_BT))$ is the dimensionless force per ssDNA Kuhn segment of length b (1.5 nm).[62] In this model, we assume that the part of the chain in the peeling junction (where the links switch between adsorbed and desorbed states) is in equilibrium. Given the contour length of ssDNA monomer, (b_{mono} = 0.56 nm),[22] one can calculate its free energy of binding per nucleotide, $\gamma' b_{mono} = \Gamma' k_BT(b_{mono}))/b)$,[36] by using the measured peeling forces, f. Furthermore, to account for the enthalpic stretching of the ssDNA, we used a corrected model (extendable FJC) to calculate the dimensionless peeling forces:[22]

dx.doi.org/10.1021/ja5055498 | J. Am. Chem. Soc. 2014, 136, 12947−12957

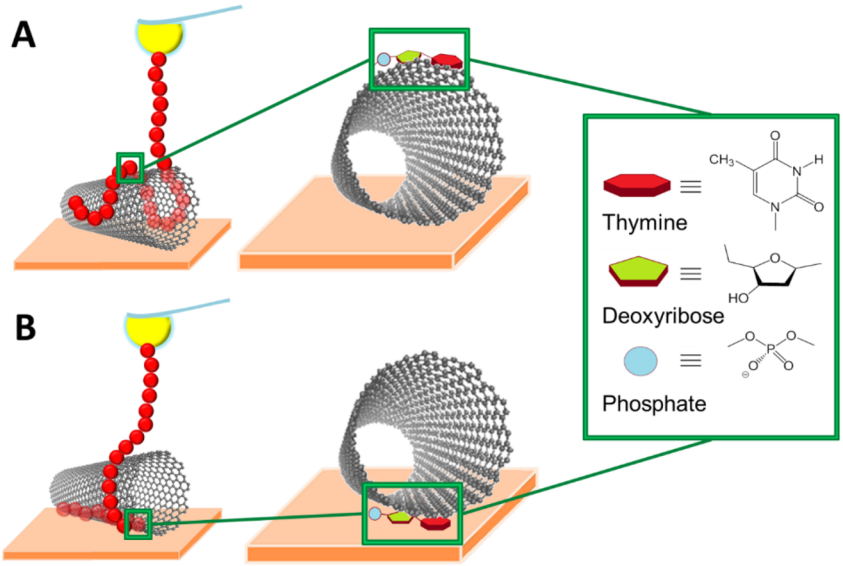

Figure 8. Pictorial representation of proposed hypotheses to explain the enhanced interaction between ssDNA and SWCNTs, compared to ssDNA with graphite. (A) ssDNA has a natural curvature that leads to preferred adsorption on the curved surface of an SWCNT. (B) ssDNA intercalates between the SWCNT and the hydrophobic substrate.[26]

$$F = \frac{fb\left(1 + \frac{f}{k}\right)}{k_B T} \quad (2)$$

Here, κ is the segment elasticity of ssDNA (κ = 2.4 nN).

By comparing the mean free energy of binding per nucleotide required to remove ssDNA homopolymers, we rank the interaction of these sequences with SAM substrates in the following order, A > G ≈ T > C, which is quite different from the interaction of the same molecules with HOPG, T ≥ A > G ≥ C.[36] In addition to differences in rank order, the surface curvature of the deposited SWCNTs appears to affect the intramolecular interactions and the formation of secondary structures by the ssDNA homopolymers. For example, we previously observed a bimodal peeling force distribution when peeling G_{100} from HOPG. In those studies, the population of high force interactions, absent in experiments on any of the other three homopolymers, was associated with the formation of secondary structures by poly(G), since it is unique among the four homopolymers in its ability to form stable secondary structures in solution (G-quadruplexes). The studies discussed in this paper show a bimodal distribution of forces for all homopolymers when they are peeled off a surface that is partly covered by deposited SWCNTs, and we have shown that the population of high peeling forces corresponds to interaction with SWCNTs. All homopolymers show a single peak for peeling force distributions characterizing interactions between ssDNA and SAM surfaces suggestive of diminished formation of secondary structures in G_{100}. Furthermore, with the exception of A_{100}, we have found that the peeling forces of ssDNA from the hydrophobic SAM surfaces are quite similar in magnitude (74−78 pN) to those we previously measured using HOPG as the solid substrate (65−80 pN). The combination of these results thus shows that the SWCNTs' surface curvature plays a fairly complex role. Also, the chemical nature of the substrate and effect of the phosphodiester backbone are reflected in the ranking of the strength of the DNA−surface interactions, which do not always trace the trends expected on the basis of the size of the nucleobases (i.e., the forces do not scale with the footprint of the hydrophobic contact).

With the exception of adenine, interaction energy between SAM and all nucleotides is very similar. The relative order of the DNA binding strength for SWCNT is the same as for SAM (A > G > T > C); however, the differences between different nucleotides are much more pronounced than in the case of flat nonpolar surfaces (SAM and graphite). This ranking reflects the relative size of the nucleobases and agrees with the theoretical and experimental results on adsorption energies of monomeric nucleobases.[22,63−65] Quantum mechanical studies on DNA nucleobases physisorbed on carbon surfaces have shown an inverse relationship between their free energy of binding (in vacuum) and the curvature of the carbon nanotube.[66] This finding is consistent with the expectation that the π-stacking (or van der Waals) interactions between the DNA's aromatic nucleobases and an aromatic surface should decrease with an increase in surface curvature, i.e., going from graphite to carbon nanotubes. However, our experimental results are in stark contrast to this expectation, demonstrating that the interaction of the ssDNA with surface-adsorbed SWCNTs is much stronger than with flat graphite.

3.3. Molecular Simulation Results. The experimental results show that ssDNA binds to SWCNTs with strength roughly twice as great as that to flat graphite. The results of molecular simulations allow us to examine the plausibility of several hypotheses and to understand the origin of this unexpected enhancement in binding. Because the adsorption free energy is about 10 k_BT per base, it is not feasible even with extensive REMD simulation to obtain equilibrium ensembles of adsorbed versus desorbed structures. However, because barriers for lateral motion of adsorbed structures are relatively small,[67] REMD allows essentially complete sampling of various adsorbed conformations, yielding robust information about equilibrium adsorbed ensembles.

As depicted in Figure 8A, one possibility is that this enhancement in interactions is indicative of a spontaneous or intrinsic curvature that the ssDNA backbone prefers to adopt. This natural curvature of the ssDNA matches the radius of the

dx.doi.org/10.1021/ja5055498 | J. Am. Chem. Soc. 2014, 136, 12947−12957

SWCNT. For example, Takahashi et al. have shown that carbon nanotubes can disentangle the agglomerated structure that DNA takes in solution while HOPG cannot do so.[68]

An alternative hypothesis is that the increase in the peeling forces of ssDNA homopolymers from SWCNTs (compared to graphite) is due to the preference of the hydrophobic bases to minimize their interactions with the surrounding aqueous buffer solution (Figure 8B). In order to gain the most favorable interaction, these amphiphilic molecules may be repositioning themselves to insert the bases into the hydrophobic SAM−SWCNT interface, while keeping polar and charged backbone exposed to highly polar aqueous environment. Since, experimentally, free energy of binding to SAM and graphite are similar in magnitude, the intercalation of nucleobases between SWCNT and SAM surface would be consistent with approximately doubling of apparent free energy of binding when moving from flat surfaces of SAM or graphite to a sample of nanotubes residing on the methyl surface.

In principle, one should also consider the possibility that DNA strands can insert inside the nanotube. Experiments on pulling DNA from the nanotube pores demonstrate much higher steady state forces that what we typically observed for peeling ssDNA from graphite.[26,69] However, several observations would contradict this interpretation. Many nanotubes shown in Figure 7 are 500 nm or greater in length. The length of the DNA used to produce this force−volume map is about 60 nm. In spite of this order of magnitude disparity in length, we observed high peeling forces along the entire axis of these long nanotubes and not only at the end points where DNA entry inside the nanotubes is possible. In addition, limiting presumed active sites for strong SWCNT−DNA interactions to nanotube ends should greatly reduce the relative frequency of observing high forces. Thus, corresponding peak area would not reflect apparent surface coverage, an effect we do not observe.

Figure 9 shows results from REMD simulation of T_{12} ssDNA and a (6,5) SWCNT in a solvated box in the vicinity of a methyl-terminated SAM surface. Figure 9 A,B shows a typical conformation from the largest cluster. Given the opportunity to choose between the SAM surface and the SWCNT, all clusters show that the DNA has a strong preference for adsorption to the SWCNT surface, which is consistent with the experimental finding that the force required to peel the molecule off SWCNTs is significantly larger than that needed to remove them from the SAM surface. We saw no evidence of DNA strands lying parallel to the SWCNT axis so that a significant fraction of bases could be inserted between the SWCNT and the SAM surface. Occasionally, one or two bases could be found close to the interface where SWCNT surface meets the SAM surface. These observations appear to rule out the second hypothesis: that peel forces are higher on the SWCNT because bases intercalate between the hydrophobic SWCNT and the SAM surface. Figure 9C shows a map of density as a function of distance along a direction normal to the SAM surface. It shows that the DNA is bound to the SWCNT and partly to the adjacent SAM surface but does not intercalate between the SWCNT and the SAM.

Figure 10 shows the results of three control REMD simulations. Figure 10E shows a conformation (from the largest cluster) from a simulation of T_{12} ssDNA and a (6,5)-SWCNT near a graphite surface. This situation corresponds to the case shown in Figure 9, but with the SAM layer replaced by graphite. In all cases, we observe that at least part of the DNA is

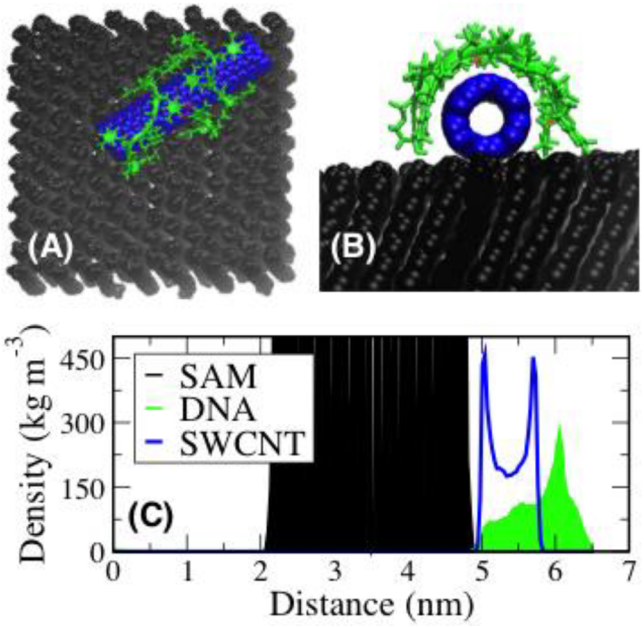

Figure 9. (A) Typical conformation from the most populated cluster based on equilibrium ensemble at 300 K obtained by REMD simulation. Hydrogen bonds based on distance less than 3.5 Å between donor and acceptor atoms and acceptor−hydrogen−donor angle greater than 30° are highlighted by dashed red lines. (B) Alternate view of the conformation shown in part A. (C) Density map as a function of distance along a direction normal to the SAM surface shows that the DNA is bound to the SWCNT and partly to the adjacent SAM surface but does not intercalate between the SWCNT and the SAM.

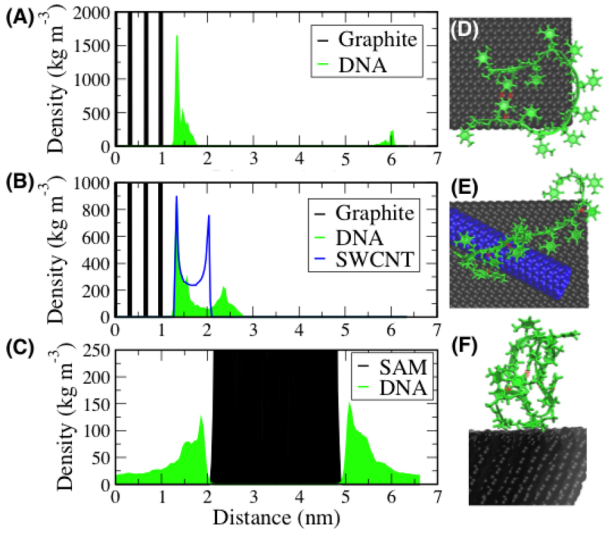

Figure 10. Results of control REMD simulations. Density profiles in the case of (A) DNA on a graphite surface, (B) DNA and SWCNT on a graphite surface, (C) DNA on a methyl-terminated SAM, and respective conformations selected from the top cluster are shown in parts D−F as right-hand side panels.

adsorbed around the SWCNT, but unlike in the case of the SAM substrate, a substantial part of the DNA is also adsorbed directly onto the graphitic surface (see Figure 10B). From this observation we can conclude that the DNA does prefer the curved SWCNT surface, albeit not dominantly as in the case of a SAM substrate, thus partially supporting our first hypothesis.

dx.doi.org/10.1021/ja5055498 | J. Am. Chem. Soc. 2014, 136, 12947−12957

Figure 10D,F shows the largest clusters of conformations for DNA on graphite and the SAM surface, respectively, in the absence of an SWCNT. We find that, nearly in all cases, the DNA bases all adsorb onto the graphitic surface whereas only some do so on the SAM surface. Figure 10 A,C shows DNA density distributions in the vicinity of the two surfaces, indicating again that the DNA is more tightly adsorbed to the graphitic surface than to the SAM. In particular, it appears that adsorption onto the SAM has to compete with hydrogen bonding and stacking interactions between the DNA bases.

If we use the fraction of DNA adsorbed on SWCNT versus the flat surface as a measure of affinity of ssDNA to corresponding substrates, then graphite shows a higher binding affinity than the SAM surface according to the preferred structures in Figures 9 A and 10 E. However, even in the case of SWCNT on graphite, the DNA exhibits a preference for the curved SWCNT surface. To quantify this preference, we calculate the accessible surface areas of the graphite and the SWCNT. The graphite surface area is determined from the simulation box dimensions in the *xy* plane and the surface area of the cylindrical SWCNT from its diameter and length. DNA is excluded from adsorption on the part of the surface area of graphite and SWCNT near nanotube−graphite contact. The inaccessibility to DNA of the graphite and SWCNT surfaces due to their close proximity around contact region is not straightforward to quantify as it depends on DNA conformation (radius of gyration and shape). We subtract equal amounts of area from the graphite and SWCNT, equal to $^1/_4$ of the SWCNT surface area, as not accessible to DNA. The result is that accessible SWCNT surface area is 22% of the total area available for adsorption. We calculated the number of DNA bases adsorbed on the SWCNT, on the basis of the distance cutoff between a heavy atom of a DNA base and carbon atoms of the graphite or SWCNT. If more than 5 heavy atoms (out of a total of 9) are in contact, based on a 5 Å distance cutoff, we label this base as adsorbed. We find that 48% of bases are adsorbed on the SWCNT, and 56% are adsorbed on the graphite, averaged over the entire simulation trajectory (these percentages do not add up to 100% because a small fraction is found to be adsorbed to both the SWCNT and the graphite, based on our definition). After correcting for the difference in accessible area, this classification results in approximately a 3:1 ratio of the SWCNT-to-graphite bound fractions. More extensive modeling that significantly expands the system size to more accurately reflect experimental settings and can provide a direct estimate of ssDNA binding strength may be needed to achieve quantitative agreement between our experiments and simulations in defining the differences in ssDNA affinity for the three nonpolar surfaces.

4. CONCLUSIONS

We have used single molecule force spectroscopy to measure the force required to remove each of the four ssDNA homopolymers from surface-adsorbed single-walled carbon nanotubes as well as from a methyl-terminated self-assembled monolayer. We have shown that free energy of binding of these ssDNA sequences to the SAM-modified substrate is quite similar to their free energy of binding to graphite. We discovered that, contrary to the expectation that the binding of ssDNA with carbon surfaces should decrease with surface curvature, the peeling forces in fact are greater by a factor of 2−3 in our measurements on SWCNTs. Supported by REMD simulations, we interpret the enhancement in this binding to result, at least partially, from spontaneous curvature of ssDNA or preference of the ssDNA to adopt highly curved conformation when adsorbed on nonpolar surfaces. It is also possible that there are additional contributions to the difference in peeling force between graphite and SWCNTs that reflect intrinsic differences in binding of bases to these two entities. There are indications from REMD simulations that these differences could result from the ability to form intrastrand hydrogen bonds in the most probable conformation of ssDNA on curved and flat surfaces.

AUTHOR INFORMATION

Corresponding Authors

dvezenov@lehigh.edu
anj6@lehigh.edu

Notes

The authors declare no competing financial interest.

ACKNOWLEDGMENTS

This work was supported by the National Science Foundation through Grant CMMI-1014960. The use of the high-performance computing capabilities of the Extreme Science and Engineering Discovery Environment (XSEDE) through grants MCB-120014 (J.M.) and TG-MCB100049 (A.J.), is also gratefully acknowledged. J.M. is grateful to Professor Shekhar Garde for providing the self-assembled monolayer surface parameters. We would like to thank Dr. Rob Pafchek for assistance with acquisition and analysis of the XPS data, and Dr. Constantine Khripin for his guidance with making SAMs and sample preparation.

REFERENCES

(1) Zhang, J.; Boghossian, A. A.; Barone, P. W.; Rwei, A.; Kim, J.-H.; Lin, D.; Heller, D. A.; Hilmer, A. J.; Nair, N.; Reuel, N. F.; Strano, M. S. *J. Am. Chem. Soc.* **2010**, *133*, 567.
(2) Liu, Z.; Sun, X.; Nakayama-Ratchford, N.; Dai, H. *ACS Nano* **2007**, *1*, 50.
(3) Popov, A. M.; Lozovik, Y. E.; Fiorito, S.; Yahia, L. *Int. J. Nanomed.* **2007**, *2*, 361.
(4) Tu, X.; Manohar, S.; Jagota, A.; Zheng, M. *Nature* **2009**, *460*, 250.
(5) Tasis, D.; Tagmatarchis, N.; Georgakilas, V.; Prato, M. *Chem.—Eur. J.* **2003**, *9*, 4000.
(6) Balasubramanian, K.; Burghard, M. *Small* **2005**, *1*, 180.
(7) Ghosh, S.; Rao, C. *Nano Res.* **2009**, *2*, 183.
(8) Moore, V. C.; Strano, M. S.; Haroz, E. H.; Hauge, R. H.; Smalley, R. E.; Schmidt, J.; Talmon, Y. *Nano Lett.* **2003**, *3*, 1379.
(9) Manna, A. K.; Pati, S. K. *J. Mater. Chem. B* **2013**, *1*, 91.
(10) Zheng, M.; Jagota, A.; Semke, E. D.; Diner, B. A.; Mclean, R. S.; Lustig, S. R.; Richardson, R. E.; Tassi, N. G. *Nat. Mater.* **2003**, *2*, 338.
(11) Zheng, M.; Jagota, A.; Strano, M. S.; Santos, A. P.; Barone, P.; Chou, S. G.; Diner, B. A.; Dresselhaus, M. S.; Mclean, R. S.; Onoa, G. B.; Samsonidze, G. G.; Semke, E. D.; Usrey, M.; Walls, D. J. *Science* **2003**, *302*, 1545.
(12) Dieckmann, G. R.; Dalton, A. B.; Johnson, P. A.; Razal, J.; Chen, J.; Giordano, G. M.; Muñoz, E.; Musselman, I. H.; Baughman, R. H.; Draper, R. K. *J. Am. Chem. Soc.* **2003**, *125*, 1770.
(13) Grigoryan, G.; Kim, Y. H.; Acharya, R.; Axelrod, K.; Jain, R. M.; Willis, L.; Drndic, M.; Kikkawa, J. M.; DeGrado, W. F. *Science* **2011**, *332*, 1071.
(14) Zorbas, V.; Ortiz-Acevedo, A.; Dalton, A. B.; Yoshida, M. M.; Dieckmann, G. R.; Draper, R. K.; Baughman, R. H.; Jose-Yacaman, M.; Musselman, I. H. *J. Am. Chem. Soc.* **2004**, *126*, 7222.
(15) Zhao, Y.-L.; Stoddart, J. F. *Acc. Chem. Res.* **2009**, *42*, 1161.
(16) Notley, S. M.; Norgren, M. *Holzforschung* **2012**, *66*, 615.

(17) Valle-Delgado, J. J.; Urban, P.; Fernandez-Busquets, X. *Nanoscale* **2013**, *5*, 3673.
(18) Hugel, T.; Grosholz, M.; Clausen-Schaumann, H.; Pfau, A.; Gaub, H.; Seitz, M. *Macromolecules* **2001**, *34*, 1039.
(19) Li, H.; Cao, Y. *Acc. Chem. Res.* **2010**, *43*, 1331.
(20) Sbrana, F.; Lorusso, M.; Canale, C.; Bochicchio, B.; Vassalli, M. *J. Biomech.* **2011**, *44*, 2118.
(21) Martines, E.; Zhong, J.; Muzard, J.; Lee, A. C.; Akhremitchev, B. B.; Suter, D. M.; Lee, G. U. *Biophys. J.* **2012**, *103*, 649.
(22) Manohar, S.; Mantz, A. R.; Bancroft, K. E.; Hui, C.-Y.; Jagota, A.; Vezenov, D. V. *Nano Lett.* **2008**, *8*, 4365.
(23) Kotamarthi, H. C.; Sharma, R.; Narayan, S.; Ray, S.; Ainavarapu, S. R. K. *J. Am. Chem. Soc.* **2013**, *135*, 14768−14774.
(24) Bujalowski, P. J.; Oberhauser, A. F. *Methods (Amsterdam, Neth.)* **2013**, *60*, 151.
(25) Stahl, S. W.; Puchner, E. M.; Alexandrovich, A.; Gautel, M.; Gaub, H. E. *Biophys. J.* **2011**, *101*, 1978.
(26) Lulevich, V.; Kim, S.; Grigoropoulos, C. P.; Noy, A. *Nano Lett.* **2011**, *11*, 1171.
(27) Arnold, M. S.; Green, A. A.; Hulvat, J. F.; Stupp, S. I.; Hersam, M. C. *Nat. Nanotechnol.* **2006**, *1*, 60.
(28) Shankar, A.; Jagota, A.; Mittal, J. *J. Phys. Chem. B* **2012**, *116*, 12088.
(29) Lee, J.-H.; Choi, Y.-K.; Kim, H.-J.; Scheicher, R. H.; Cho, J.-H. *J. Phys. Chem. C* **2013**, *117*, 13435.
(30) Fisher, T. E.; Oberhauser, A. F.; Carrion-Vazquez, M.; Marszalek, P. E.; Fernandez, J. M. *Trends Biochem. Sci.* **1999**, *24*, 379.
(31) Best, R. B.; Clarke, J. *Chem. Commun.* **2002**, 183.
(32) Rief, M.; Grubmüller, H. *ChemPhysChem* **2002**, *3*, 255.
(33) Zlatanova, J.; Lindsay, S. M.; Leuba, S. H. *Prog. Biophys. Mol. Biol.* **2000**, *74*, 37.
(34) Ducker, W. A.; Senden, T. J.; Pashley, R. M. *Nature* **1991**, *353*, 239.
(35) Manohar, S.; Mantz, A.; Hui, C.-Y.; Jagota, A.; Vezenov, D. V. *Nano Lett.* **2008**, *8*, 4365.
(36) Iliafar, S.; Wagner, K.; Manohar, S.; Jagota, A.; Vezenov, D. *J. Phys. Chem. C* **2012**, *116*, 13896.
(37) Wei, G.; Li, Q.; Steckbeck, S.; Ciacchi, L. C. *Phys. Chem. Chem. Phys.* **2014**, *16*, 3995.
(38) Wei, G.; Steckbeck, S.; Köppen, S.; Ciacchi, L. C. *Chem. Commun.* **2013**, *49*, 3239.
(39) Friedsam, C.; Gaub, H. E.; Netz, R. R. *Europhys. Lett.* **2005**, *72*, 844.
(40) Elder, R. M.; Jayaraman, A. *Soft Matter* **2013**, *9*, 11521.
(41) Manna, A. K.; Pati, S. K. *J. Mater. Chem. B* **2013**, *1*, 91.
(42) Tu, X.; Manohar, S.; Jagota, A.; Zheng, M. *Nature* **2009**, *460*, 250.
(43) Roxbury, D.; Mittal, J.; Jagota, A. *Nano Lett.* **2012**, *12*, 1464.
(44) Iliafar, S.; Vezenov, D.; Jagota, A. *Langmuir* **2013**, *29*, 1435.
(45) Paturej, J.; Dubbeldam, J. L.; Rostiashvili, V. G.; Milchev, A.; Vilgis, T. A. *Soft Matter* **2014**, *10*, 2785.
(46) Khripin, C. Y.; Zheng, M.; Jagota, A. *J. Colloid Interface Sci.* **2009**, *330*, 255.
(47) Huang, X.; Kovaleski, J. M.; Wirth, M. J. *Anal. Chem.* **1996**, *68*, 4119.
(48) Roxbury, D.; Tu, X.; Zheng, M.; Jagota, A. *Langmuir* **2011**, *27*, 8282.
(49) Sugita, Y.; Okamoto, Y. *Chem. Phys. Lett.* **1999**, *314*, 141.
(50) Hess, B.; Kutzner, C.; Van Der Spoel, D.; Lindahl, E. *J. Chem. Theory Comput.* **2008**, *4*, 435.
(51) Foloppe, N.; MacKerell, A. D. *J. Comput. Chem.* **2000**, *21*, 86.
(52) Jorgensen, W. L.; Chandrasekhar, J.; Madura, J. D.; Impey, R. W.; Klein, M. L. *J. Chem. Phys.* **1983**, *79*, 926.
(53) Jamadagni, S. N.; Godawat, R.; Garde, S. *Langmuir* **2009**, *25*, 13092.
(54) Godawat, R.; Jamadagni, S. N.; Garde, S. *Proc. Natl. Acad. Sci. U.S.A.* **2009**, *106*, 15119.
(55) Alexiadis, A.; Kassinos, S. *Chem. Rev.* **2008**, *108*, 5014.
(56) Nosé, S. *Mol. Phys.* **1984**, *52*, 255.
(57) Hoover, W. G. *Phys. Rev. A* **1985**, *31*, 1695.
(58) Essmann, U.; Perera, L.; Berkowitz, M. L.; Darden, T.; Lee, H.; Pedersen, L. G. *J. Chem. Phys.* **1995**, *103*, 8577.
(59) Daura, X.; Gademann, K.; Jaun, B.; Seebach, D.; van Gunsteren, W. F.; Mark, A. E. *Angew. Chem., Int. Ed.* **1999**, *38*, 236.
(60) Ptasinska, S.; Stypczynska, A.; Nixon, T.; Mason, N. J.; Klyachko, D. V.; Sanche, L. *J. Chem. Phys.* **2008**, *129*, 065102.
(61) Kendall, K. *J. Phys. D: Appl. Phys.* **1975**, *8*, 1449.
(62) Smith, S. B.; Cui, Y.; Bustamante, C. *Science* **1996**, *271*, 795.
(63) Paik, D. H.; Perkins, T. T. *Angew. Chem., Int. Ed.* **2012**, *51*, 1811.
(64) Krautbauer, R.; Pope, L. H.; Schrader, T. E.; Allen, S.; Gaub, H. E. *FEBS Lett.* **2002**, *510*, 154.
(65) Chaurasiya, K. R.; Paramanathan, T.; McCauley, M. J.; Williams, M. C. *Phys. Life Rev.* **2010**, *7*, 299.
(66) Umadevi, D.; Sastry, G. N. *J. Phys. Chem. Lett.* **2011**, *2*, 1572.
(67) Wells, D. B.; Belkin, M.; Comer, J.; Aksimentiev, A. *Nano Lett.* **2012**, *12*, 4117.
(68) Takahashi, H.; Numao, S.; Bandow, S.; Iijima, S. *Chem. Phys. Lett.* **2006**, *418*, 535.
(69) Roxbury, D.; Jagota, A.; Mittal, J. *J. Phys. Chem. B* **2013**, *117*, 132.